

# Journal of Materials Chemistry A

Accepted Manuscript



This is an *Accepted Manuscript*, which has been through the Royal Society of Chemistry peer review process and has been accepted for publication.

*Accepted Manuscripts* are published online shortly after acceptance, before technical editing, formatting and proof reading. Using this free service, authors can make their results available to the community, in citable form, before we publish the edited article. We will replace this *Accepted Manuscript* with the edited and formatted *Advance Article* as soon as it is available.

You can find more information about *Accepted Manuscripts* in the [Information for Authors](#).

Please note that technical editing may introduce minor changes to the text and/or graphics, which may alter content. The journal's standard [Terms & Conditions](#) and the [Ethical guidelines](#) still apply. In no event shall the Royal Society of Chemistry be held responsible for any errors or omissions in this *Accepted Manuscript* or any consequences arising from the use of any information it contains.

## Zn-doped Ni-MOF material with a high supercapacitive performance

Cite this: DOI: 10.1039/x0xx00000x

Jie Yang,<sup>a, b</sup> Cheng Zheng<sup>a, b</sup> Peixun Xiong,<sup>a, b</sup> Yafeng Li<sup>a, b</sup> and Mingdeng Wei<sup>\* a, b</sup>

Received 00th January 2012,  
Accepted 00th January 2012

DOI: 10.1039/x0xx00000x

[www.rsc.org/](http://www.rsc.org/)

A layered structural Zn-doped Ni-MOF was synthesized and, for the first time, used as an electrode material for a supercapacitor. It exhibited large specific capacitance, high rate capability and good cycling stability. Capacitances of 1620 and 854 F g<sup>-1</sup> can be achieved at rates of 0.25 and 10 A g<sup>-1</sup>, respectively. At the same time, the retention was kept at over 91% even after 3000 cycles. These values demonstrated the best performance of all the MOF materials in supercapacitor at present. Such an excellent electrochemical property may be attributed to the intrinsic characteristics of Zn-doped Ni-MOF material including its crystal structure and morphology.

### Introduction

The interest in energy-storage devices has boomed in recent years due to use of intermittent energy generated by green sources, longer autonomy and miniaturization of portable devices, the search for competitive cost and performance of hybrid and electric cars.<sup>1</sup> Among various energy storage systems, supercapacitors, also known as electrochemical capacitors, can store high energy and transport high power within a very short period and are therefore projected to be one of the best candidates for portable electronic devices and hybrid electric vehicles.<sup>2</sup> So far, carbon materials, transition metal oxides and conducting polymers are conventional electrode materials for supercapacitors,<sup>3, 4</sup> but their applications were restricted based on the rapid development of supercapacitor with higher performance. Thus, the development of newly advanced electrode materials with high performance for supercapacitors is essential.

Metal-organic frameworks (MOFs), also known as coordination polymers or coordination networks, have attracted tremendous attention because of their high accessible surface areas, tuneable pore sizes, open metal sites and ordered crystalline structures.<sup>5</sup> They have widely used in many aspects such as magnetism,<sup>6</sup> fluorescence,<sup>7</sup> catalysis<sup>8</sup> and so on. On the other hand, MOFs are electrochemically active materials<sup>9</sup> and have been used in the electrochemical fields including fuel cells,<sup>10</sup> lithium-ion rechargeable batteries,<sup>11</sup> supercapacitors,<sup>12</sup> solar cells,<sup>13</sup> Li-S batteries<sup>14</sup> and so on. Recently, MOFs have been used directly as electrode materials for supercapacitors and received some attention. To the best of our knowledge, however, the works by several groups are the only reports

dealing with the electrochemical properties of MOFs in supercapacitors including Zr-,<sup>15</sup> Fe-,<sup>16</sup> Co-,<sup>17, 18</sup> In-,<sup>19</sup> Co-Zn-,<sup>20</sup> Zn- and Cd-<sup>21</sup> materials. Among them, the study recently reported by Kang et al.<sup>15</sup> is with the best performance at present, in which a series of graphene-doped nMOFs (MOFs made as nanocrystals) have been used to fabricate a symmetric supercapacitor and it was found that the Zr-MOF material exhibited a high capacitance of 726 F g<sup>-1</sup> at a current density of 0.88 mA cm<sup>-3</sup> (6.95  $\mu$ A g<sup>-1</sup>). However, an organic electrolyte of (C<sub>2</sub>H<sub>5</sub>)<sub>4</sub>NBF<sub>4</sub> was used, which may lead to some issues such as insecurity, high cost, low conductivity and strict assembly process. In addition, the mass loading (0.007 mg cm<sup>-2</sup>) of the electrode film was too small and the practical application of this material will be limited. Other reports<sup>16-21</sup> generally showed very low capacitances, indicating that the present research in this field is still on an early stage. From an overall perspective, the literatures in this field are quite disperse and can be considered as limited successes due to the poor electrical conductivity, large space steric hindrance, unmatched electrolyte, and so on.<sup>22, 23</sup> Thus, it is quite necessary to find a new kind of MOF materials with a unique structure which have good conductivity, low steric hindrance and good electrolyte compatibility, ensuring the predominant charge storage mechanism can manifest through a pseudocapacitive reaction process with fast electron transfer and electrolyte diffusion, and thereby exhibiting high performance.

In our previous work,<sup>24</sup> a layered structure Ni-MOF has been chosen as a supercapacitor electrode material and exhibited large specific capacitance, high rate capability and good cycling stability. However, the maximum capacitance of 1127 F g<sup>-1</sup> was not remarkable enough for a kind of

pseudocapacitive material. To further improve the capacitance, a Zn-doped Ni-MOF was synthesized in the present work. This material was firstly used as a supercapacitor electrode and exhibited the highest electrochemical performance for all the MOF materials in supercapacitor at present. Furthermore, the relationships between the electrochemical properties and the structural characteristics of electrode material were also investigated in detail.

## Experimental

**Synthesis of MOFs.** In a typical synthesis, 0.166 g of p-benzenedicarboxylic acid (PTA), 0.096 g of  $\text{Ni}(\text{NO}_3)_2 \cdot 6\text{H}_2\text{O}$ , and different amounts of  $\text{ZnCl}_2$  (0, 0.0228, 0.0456 and 0.0912 g) were dissolved in 20 mL N, N-dimethylformamide (DMF) with stirring at room temperature. Then, 2 ml of NaOH solution (0.4 M) was slowly added to the above solution drop by drop. After that, the mixture was then transformed into a Teflon-lined stainless steel autoclave with a capacity of 40 mL. The autoclave was kept at 100 °C for 8 h and then cooled to room temperature naturally. The resulting precipitate was thoroughly washed with DMF and alcohol for several times, respectively. Finally, the green product was dried at 120 °C for 12 h in air. Herein, Zn-doped Ni-based MOF materials prepared with different amount of  $\text{ZnCl}_2$  (0, 0.0228, 0.0456 and 0.0912 g) are denoted as MOF-0, MOF-1, MOF-2 and MOF-3, respectively.

**Structural and elemental characterization.** X-ray diffraction (XRD) patterns were recorded on PANalytical X'Pert spectrometer using the  $\text{Co-K}\alpha$  radiation and the data were changed to  $\text{Cu-K}\alpha$  data. Scanning electron microscopy (SEM) and transmission electron microscopy (TEM) were taken on a Hitachi S4800 instrument and a FEI F20 S-TWIN instrument, respectively. Surface area was determined by Brunauer–Emmet–Teller (BET) method using ASAP2020 from Quanta Chrome. Initially, the sample was vacuum degassed for 6 h at 150 °C under the flow of nitrogen before the BET measurement. Fourier Transform Infrared (FT-IR) transmission spectra were taken on a BRUKER-EQUINOX-55 IR spectrophotometer. Thermo Gravimetric-Differential Thermal Analysis (TG-DTA) was performed using the Setsys Evolution instrumentation with a rate of 10 °C  $\text{min}^{-1}$  under ambient conditions. X-ray photoelectron spectroscopy (XPS) measurements (ESCALAB 250) were performed to analyze the surface species and their chemical states.

**Electrochemical measurements.** Electrochemical properties of the samples were evaluated in a standard three electrode test pool (Hangzhou Saiao Electrochemistry Technology Co., Ltd). For the working electrode, a mixture containing of 70 wt. % active material, 20 wt. % acetylene black, and 10 wt. % PTFE binder was well mixed. Then the mixture was pressed with several drops of isopropyl alcohol solvent to form a thin sheet. The sheet was rolled to get approximate thickness of 100  $\mu\text{m}$  and then pressed onto a stainless steel mesh. The mass loading of the sample Ni-MOF is about 5  $\text{mg cm}^{-2}$ . Platinum foil and saturated calomel electrode were used as the counter and

reference electrodes, respectively. The electrolyte was 6 M KOH. Cyclic voltammetry (CV), galvanostatic charge-discharge (GCD) measurements, electrochemical impedance spectroscopy (EIS) were performed on an Electrochemical Workstation (Zahner, IM6). The EIS data was collected with an AC voltage of 10 mV amplitude in the frequency range from 1 MHz to 100 mHz.

## Results and discussion

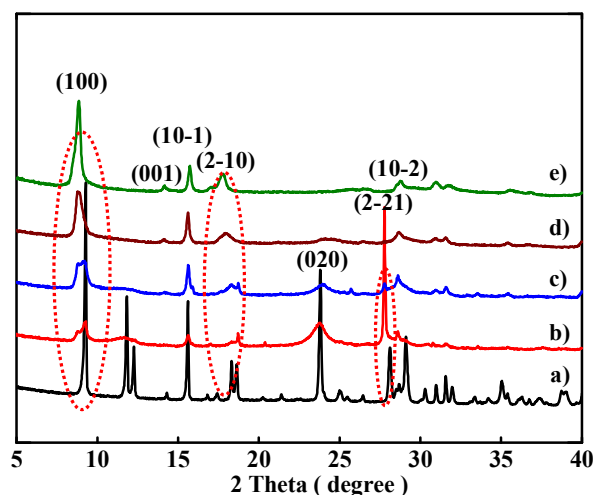


Fig. 1 XRD patterns of Zn-doped Ni-MOF materials: (a) Ni-MOF-simulation, (b) MOF-0, (c) MOF-1, (d) MOF-2 and (e) MOF-3.

Fig.1 shows the XRD patterns of the Zn-doped MOF samples. With increasing Zn amount, similarities among all the patterns were evident, suggesting that all MOFs probably had a layered topology of  $[\text{Ni}_3(\text{OH})_2(\text{C}_8\text{H}_4\text{O}_4)_2(\text{H}_2\text{O})_4] \cdot 2\text{H}_2\text{O}$  (CCDC No.638866). At the same time, some differences among them were also observed. Apart from the presence/absence of some reflections, the most evident difference was the significant  $2\theta$  shifts towards a lower angle side which was similar to the previous reports on MOFs' substitution.<sup>25-27</sup> The higher the doping amount, the bigger the shift was. This might be attributed to the fact that the larger  $\text{Zn}^{2+}$  ions (0.074 nm) replaced or partly replaced the smaller  $\text{Ni}^{2+}$  ions (0.065 nm).

SEM images of the MOF materials are depicted in Fig. 2. As presented in Fig. 2a, a great number of nanosheets were observed for the sample MOF-0. The thickness of these nanosheets was found to be about 10 nm (Fig. S1a). After the  $\text{Zn}^{2+}$  ions were introduced, the flower-like microspheres were formed, as shown in Fig. 2b. It was found that the flower-like microspheres on a large scale can be obtained in an initial solution containing suitable amount of  $\text{Zn}^{2+}$  ions, as depicted in Fig. 2c and Fig. S1b. The size of the microspheres increased apparently with increasing  $\text{Zn}^{2+}$  content in the reaction system, as shown in Fig. 2d. Therefore, the morphology of MOFs was influenced significantly in the presence of  $\text{Zn}^{2+}$  in the reaction solution, which is similar to that in a previous report on Ni-doped  $\text{Cd}_{0.1}\text{Zn}_{0.9}\text{S}$  solid solution.<sup>28</sup> In addition, the SAED patterns in the insets of Fig. 2 exhibited some diffraction spots

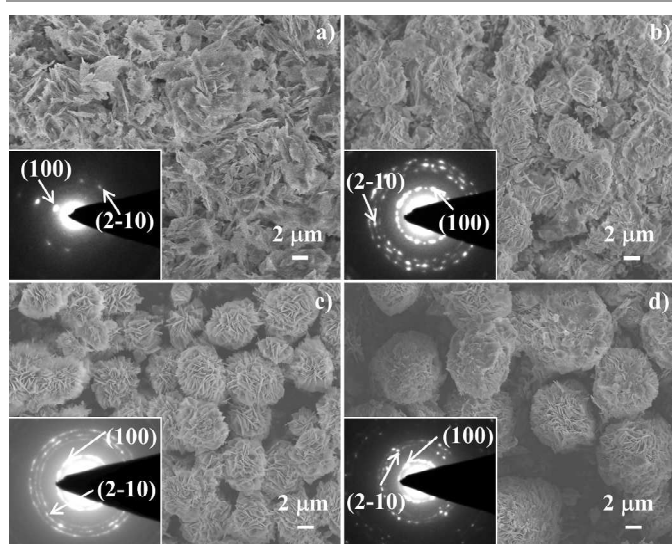


Fig. 2 SEM images of Zn-doped Ni-MOF materials: (a) MOF-0, (b) MOF-1, (c) MOF-2 and (d) MOF-3 (insets: the corresponding SAED patterns).

or spot-connected rings, which can be indexed to the (100) and (2-10) planes of the corresponding materials. It was found that the lattice distances of the two marked planes were increased with the increasing of Zn content (Table S1). This was in good agreement with the  $2\theta$  shifts in XRD patterns.

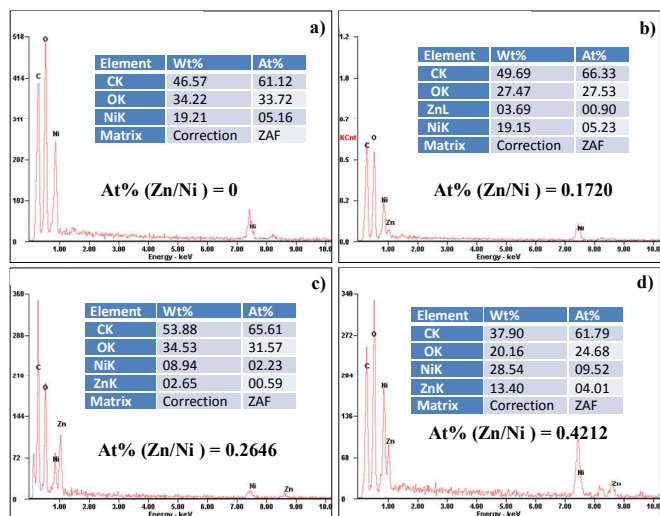


Fig. 3 EDX spectra of Zn-doped Ni-MOF materials: (a) MOF-0, (b) MOF-1, (c) MOF-2 and (d) MOF-3.

Fig.3 shows the EDX spectra of four samples of MOF materials. Zn was detected in the three Zn-doped MOF materials, indicating the presence of doping element. EDX spectra reveal that the ratios of Zn/Ni in three samples were 0.17, 0.26 and 0.42, respectively. The presence of doping element can further be confirmed by XPS measurement. As depicted in Fig.4a, no characteristic peaks in the Zn 2p spectrum was detected for MOF-0. However, three samples exhibited intense responses which can be deconvoluted into two main doublet peaks, as shown in Fig. 4b-d. The binding energies at 1021.86/1021.74 and 1044.90/1044.78 eV were

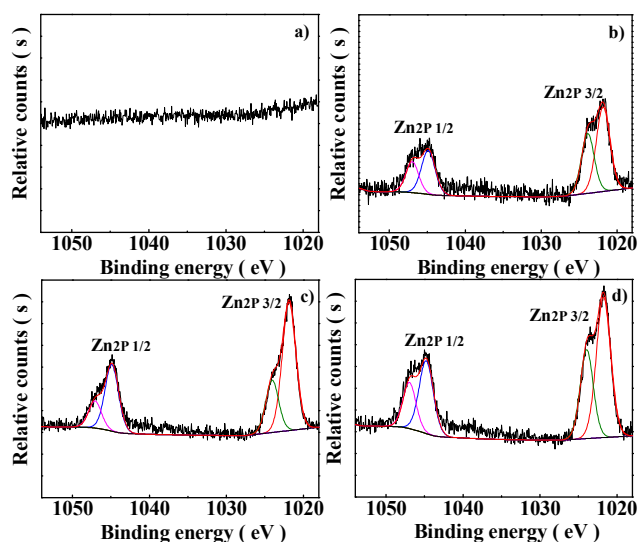


Fig. 4 Zn 2p spectra of Zn-doped Ni-MOF materials: (a) MOF-0, (b) MOF-1, (c) MOF-2 and (d) MOF-3.

assigned to Zn 2p<sub>3/2</sub> and Zn 2p<sub>1/2</sub>, respectively, indicating the presence of the coordination of ligand BDC (benzenedicarboxylic) with Zn in the Zn-doped samples.<sup>29, 30</sup> The additional two peaks observed at lower binding energy indicated that Zn was presented in two chemical environments in the Zn-doped samples.<sup>31, 32</sup> This may be related to two kinds of chemical environments around Ni in the Ni-based MOF material without doping. These results confirmed the strong chemical coordination of Zn with the Ni-MOF within the doped samples.

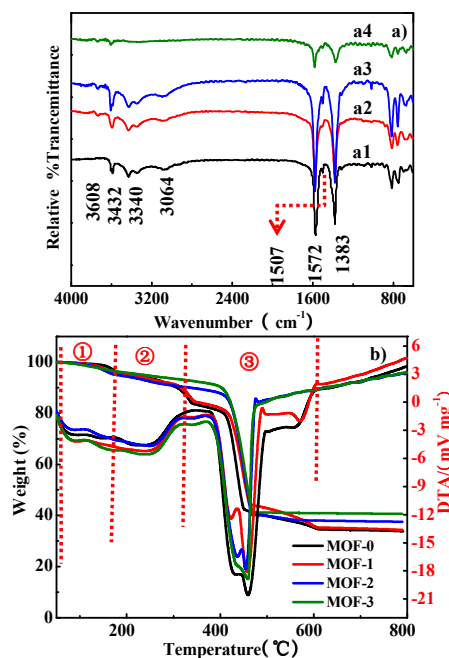


Fig.5 (a) IR spectra of Zn-doped Ni-MOF materials: (a1) MOF-0, (a2) MOF-1, (a3) MOF-2 and (a4) MOF-3, and (b) TG-DTA curves of Zn-doped Ni-MOF materials.

FTIR spectra of the MOF samples are shown in Fig. 5a. The bands at  $\sim 3608$  and  $1507\text{ cm}^{-1}$  were respectively attributed to the stretching vibrations of  $\text{OH}^-$  and *para*-aromatic CH groups. The stretching vibrations of water molecules were at around  $3432$ ,  $3340$  and  $3064\text{ cm}^{-1}$ , indicating that the coordinated  $\text{H}_2\text{O}$  molecules existed within these materials. The strong bands at  $1572$  and  $1383\text{ cm}^{-1}$  were assigned to the asymmetric and symmetric stretching modes of the coordinated ( $-\text{COO}^-$ ) group, respectively.<sup>33, 34</sup> Although the spectra for MOF-1, MOF-2 and MOF-3 exhibited almost same peak position, the wavenumber separation between the asymmetric and symmetric stretching modes of the coordinated ( $-\text{COO}^-$ ) group was slightly increased with increasing Zn content in the samples (Table S2), indicating the effect of Zn doping on their structure. TG-DTA curves of the four samples, shown in Fig. 5b, can be basically divided into three stages. The initial weight loss up to  $170\text{ }^\circ\text{C}$  was due to the loss of two solvated water molecules. The second weight loss in the range of  $170 - 300\text{ }^\circ\text{C}$  corresponded to the departure of another two solvated water molecules, while the third weight loss caused by combustion of the organic component was observed between  $300$  and  $600\text{ }^\circ\text{C}$ .<sup>35, 36</sup> It was found that all the samples showed similar curves, confirming that these samples have a similar structure. However, it also can be seen from the curves in the third stage that the effects of Zn amount on their structure still existed. These were all in good agreement with the XRD results and further confirmed that the synthesized Zn-doped MOFs were still a kind of hydroxyl-terephthalate-based compound which had a similar structure to MOF-0.

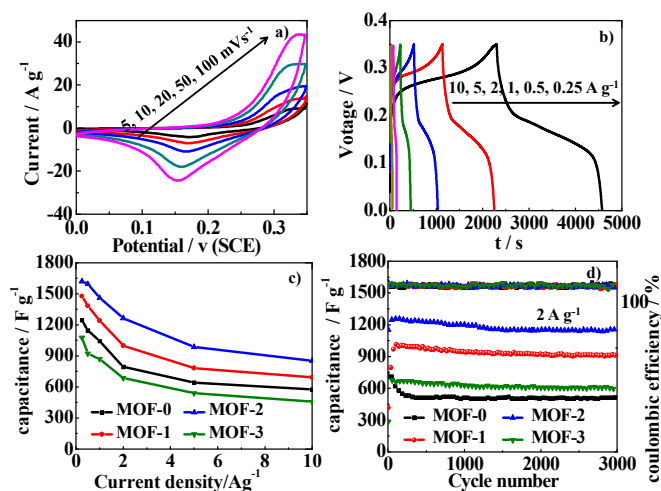
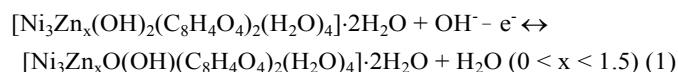


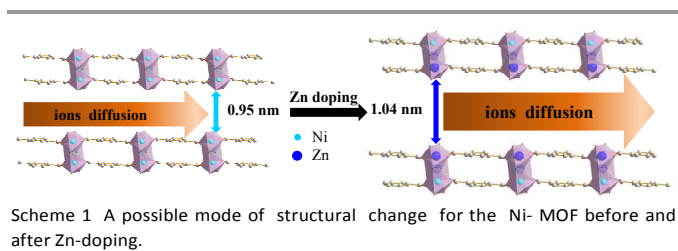
Fig. 6 Electrochemical performances of Zn-doped Ni-MOF electrodes: (a) CV curves at different scan rates for MOF-2, (b) charge-discharge profiles for MOF-2, (c) specific capacitances at different current densities, and (d) GCD cycling performance.

Fig. 6 shows the electrochemical performance for the MOFs as supercapacitor electrodes. As depicted in Fig. 6a, CV curves for the MOF-2 clearly exhibit a couple of redox peaks around  $0.33$  and  $0.15\text{ V}$  (vs. SCE), indicating that the pseudocapacitive behaviour arises from the surface faradic redox reactions. These peaks may correspond to the

intercalation and deintercalation of  $\text{OH}^-$  during electrochemical reactions based on the reports for  $\text{Ni}(\text{OH})_2$ .<sup>37, 38</sup> This process might be represented by the following equation:



Charge-discharge profiles in Fig. 6b show smoothly sloping voltage curves which were consistent with the CV results, confirming that the MOF-2 electrode had a pseudocapacitive feature.<sup>39, 40</sup> Other three MOF electrodes show the similar CV curve and charge-discharge profile (Fig. S2-S3), indicating that all the Ni-based MOFs materials with or without Zn doping were able to accommodate  $\text{OH}^-$  through pseudocapacitive processes. Capacitances at various current densities were obtained from their charge-discharge profiles and the results are presented in Fig. 6c. It can be found that the Zn-doped samples (MOF-1, MOF-2 and MOF-3) had higher capacitances than the pure Ni-based MOF (MOF-0). With increasing Zn content, the capacitance value was initially increased and then trended to decrease. A maximum specific capacitance of  $1620\text{ F g}^{-1}$  for MOF-2 was reached at a rate of  $0.25\text{ A g}^{-1}$ . Even at a current density as large as  $10\text{ A g}^{-1}$ , a capacitance of  $854\text{ F g}^{-1}$  was still retained, indicating that this material had a high rate capability. Accordingly, the maximum power and energy densities were  $1750\text{ W kg}^{-1}$  and  $27.56\text{ Wh kg}^{-1}$ , respectively. To further investigate the cycling performance, galvanostatic charge-discharge (GCD) tests were executed and the results are shown in Fig. 6d. The capacitance retentions for MOF-0, MOF-1, MOF-2 and MOF-3 were respectively kept at 66%, 92%, and 91%, 88% of their highest value after 3000 cycles, indicating that the Zn-doped Ni-MOF materials not only had a largely improved specific capacitance but also had an excellent cycling stability.



To the best of our knowledge, the present work is the first report on Zn-doped Ni-MOF used as an electrode in supercapacitor. In this case, the Zn-doped Ni-MOF materials can respectively achieve high capacitances of  $1620$  and  $860\text{ F g}^{-1}$  at  $0.25$  and  $10\text{ A g}^{-1}$ , and the capacitance loss was only 8% after 3000 cycles. These results are much better than the reported values for the Zr-based MOF material by Kang et al.<sup>15</sup> Thus, such materials really stand out in terms of their high specific capacitance, high rate capability and excellent cycling stability; this might be attributed to the intrinsic characteristics of the Zn-doped Ni-MOF including its structure and morphology. Firstly, the Zn-doped Ni-MOF has a layered structure with an enlarged interlayer distance, shown in Scheme

1, which provides an enough space for the electrolyte diffusion and ensures more facile OH<sup>-</sup> intercalation and deintercalation.<sup>41</sup> During the cycling process, the doped Zn<sup>2+</sup> will act as a pillar to prevent the collapse of crystal as doping of Zn<sup>2+</sup> in LiFePO<sub>4</sub>.<sup>42</sup> Secondly, the Zn-doped Ni-MOF materials exhibited smaller charge transfer resistances (Fig. S4), indicating faster electron transfer rate.<sup>43</sup> Thirdly, the flower-like microspheres aggregated by nanosheets can provide interconnected open pores (Fig.S5) that should be favourable for diffusion of the electrolyte<sup>44</sup> and the porous spherical structure can effectively buffer the volume variation induced during the charge-discharge process.<sup>45</sup> Therefore, such a kind of Zn-doped Ni-MOF material can exhibit an excellent electrochemical performance in supercapacitor.

## Conclusions

In summary, the Zn-doped Ni-MOFs materials with a flower-like microsphere were successfully synthesized for the first time. These microspheres were firstly used as an electrode material for supercapacitors and exhibited high specific capacitance, good rate capability and good cycling stability. For instance, the capacitances of 1620 and 860 F g<sup>-1</sup> were respectively achieved at 0.25 and 10 A g<sup>-1</sup>, and the retention was kept at 91% even after 3000 cycles for a Zn-doped Ni-MOF with a Zn/Ni of 0.26. These excellent electrochemical properties might be attributed to the intrinsic characteristics of the Zn-doped Ni-MOF including layered structure, enlarged interlayer distance and porous feature. The present studies demonstrate that such a kind of Zn-doped Ni-MOF may find applications as supercapacitor electrodes in future.

## Acknowledgements

This work was financially supported by National Natural Science Foundation of China (NSFC 21173049; J1103303; 21303020) and Research Fund for the Doctoral Program of Higher Education of China (RFDP 20133514110002).

## Notes and references

<sup>a</sup> State Key Laboratory of Photocatalysis on Energy and Environment, Fuzhou University, Fuzhou, Fujian 350002, China

<sup>b</sup> Institute of Advanced Energy Materials, Fuzhou University, Fuzhou, Fujian 350002, China

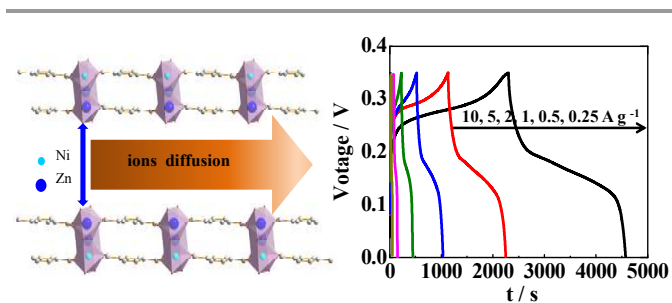
Tel./fax: +86-591-83753180; E-mail: wei-mingdeng@fzu.edu.cn

Electronic Supplementary Information (ESI) available: [details of any supplementary information available should be included here]. See DOI: 10.1039/b000000x/

- S. Chen, W. Xing, J. Duan, X. Hu and S. Z. Qiao, *J. Mater. Chem. A*, 2013, **1**, 2941.
- Z. Chang, Y. Q. Yang, M. X. Li, X. W. Wang and Y. P. Wu, *J. Mater. Chem. A*, 2014, **2**, 10739.
- J. Yang, T. B. Lan, J. D. Liu, Y. F. Song and M. D. Wei, *Electrochim. Acta*, 2013, **105**, 489.
- J. Yang, L. F. Lian, H. C. Ruan, F. Y. Xie and M. D. Wei, *Electrochim. Acta*, 2014, **136**, 189.
- S. L. James, *Chem. Soc. Rev.*, 2003, **32**, 276.
- M. Kurmoo, *Chem. Soc. Rev.*, 2009, **38**, 1353.
- L. Chen, K. Tan, Y.-Q. Lan, S.-L. Li, K.-Z. Shao and Z.-M. Su, *Chem. Commun.*, 2012, **48**, 5919.
- R.-Q. Zou, H. Sakurai, S. Han, R.-Q. Zhong and Q. Xu, *J. Am. Chem. Soc.*, 2007, **129**, 8402.
- A. Morozan and F. Jaouen, *Energy Environ. Sci.*, 2012, **5**, 9269.
- X. Q. Liang, F. Zhang, W. Feng, X. Q. Zou, C. J. Zhao, H. Na, C. Liu, F. X. Sun and G. S. Zhu, *Chem. Sci.*, 2013, **4**, 983.
- A. Banerjee, K. K. Upadhyay, D. Puthusseri, V. Aravindan, S. Madhavi and S. Ogale, *Nanoscale*, 2014, **6**, 4387.
- S. Dutta, A. Bhaumik and K. C.-W. Wu, *Energy Environ. Sci.*, 2014, Advance Article.
- A. V. Vinogradov, H. Z. Hertling, E. H. Hawkins, A. V. Agafonov, G. A. Seisenbaeva, V. G. Kessler and V. V. Vinogradov, *Chem. Commun.*, 2014, Advance Article.
- J. W. Zhou, R. Li, X. X. Fan, Y. F. Chen, R. D. Han, W. Li, J. Zheng, B. Wang and X. G. Li, *Energy Environ. Sci.*, 2014, **7**, 2715.
- K. M. Choi, H. M. Jeong, J. H. Park, Y. B. Zhang, J. K. Kang and O. M. Yaghi, *ACS nano*, 2014, **8**, 7451.
- N. Campagnol, R. Romero-Vara, W. Deleu, L. Stappers, K. Binnemans, D. E. De Vos and J. Fransaer, *ChemElectroChem*, 2014, **1**, 1182.
- D. Y. Lee, S. J. Yoon, N. K. Shrestha, S. H. Lee, H. Ahn and S. H. Han, *Microporous Mesoporous Mater.*, 2012, **153**, 163.
- D. Y. Lee, D. V. Shinde, E. K. Kim, W. Lee, I. W. Oh, N. K. Shrestha, J. K. Lee and S. H. Han, *Microporous Mesoporous Mater.*, 2013, **171**, 53.
- M. Du, M. Chen, X. G. Yang, J. Wen, X. Wang, S. M. Fang and C. S. Liu, *J. Mater. Chem. A*, 2014, **2**, 9828.
- R. Diaz, M. G. Orcajo, J. A. Botas, G. Calleja and J. Palma, *Mater. Lett.*, 2012, **68**, 126.
- Y. Gong, J. Li, P. G. Jiang, Q. F. Li and J. H. Lin, *Dalton Trans.*, 2013, **42**, 1603.
- A. Morozan and F. Jaouen, *Energy Environ. Sci.*, 2012, **5**, 9269.
- G. Combarieu, M. Morcrette, F. Millange, N. Guillou, J. Cabana, C. Grey, I. Margiolaki, G. Ferey and J. M. Tarascon, *Chem. Mater.*, 2009, **21**, 1602.
- J. Yang, P. X. Xiong, C. Zheng, H. Y. Qiu, and M. D. Wei, *J. Mater. Chem. A*, 2014, **2**, 16640.
- R. D. Shannon, *Acta Crystallogr. A Cryst. Phys.*, 1976, **32**, 751.
- K. Raju, G. Venkataiah and D. H. Yoon, *Ceram. Int.*, 2014, **40**, 9337.
- M. D. Garcia and M. S. Sánchez, *Microporous Mesoporous Mater.*, 2014, **190**, 248.
- X. H. Zhang, D. W. Jing, M. C. Liu and L. J. Guo, *Catal. Commun.*, 2008, **9**, 1720.
- L. S. Dake, D. R. Her and J. M. Zachara, *Surf. Interface Anal.*, 1989, **14**, 71.
- B. R. Strohmeier, *Surf. Sci. Spectra*, 1994, **3**, 128.
- J. Z. Chen, R. L. Liu, H. Gao, L. M. Chen and D. Q. Ye, *J. Mater. Chem. A*, 2014, **2**, 7205.
- P. Pachfule, zB. K. Balan, zS. Kurungot and R. Banerjee, *Chem. Commun.*, 2012, **48**, 2009.
- S. G. Baca, I. G. Filippova, O. A. Gherco, M. Gdaniec, Y. A. Simonov, N. V. Gerbeleu, P. Franz, R. Basler and S. Decurtins, *Inorg. Chim. Acta*, 2004, **357**, 3419.
- F. Zhang, L. Hao, L. J. Zhang and X. G. Zhang, *Int. J. Electrochem. Sci.*, 2011, **6**, 2943.

- 35 A. Carton, A. Mesbah, T. Mazet, F. Porcher and M. F. ois, *Solid State Sciences*, 2007, **9**, 465.
- 36 A. Mesbah, P. Rabu, R. Sibille, S. b. Lebegue, T. Mazet, B. Malaman and M. Francois, *Inorg. Chem.*, 2014, **53**, 872.
- 37 N. A. Alhebshi, R. B. Rakhi and H. N. Alshareef, *J. Mater. Chem. A*, 2013, **1**, 14897.
- 38 H. Wang, Y. Liang, T. Mirfakhrai, Z. Chen, H. S. Casalongue and H. Dai, *Nano Res.*, 2011, **4**, 729.
- 39 Y. Wang, Z. Hong, M. Wei and Y. Xia, *Adv. Funct. Mater.*, 2012, **22**, 5185.
- 40 J. Yang, L. F. Lian, P. X. Xiong and M. D. Wei, *Chem. Commun.*, 2014, **50**, 5973.
- 41 Y. N. Ko, S. H. Choi, S. B. Park and Y. C. Kang, *Nanoscale*, 2014, **6**, 4508.
- 42 H. Liu, Q. Cao, L. J. Fu, C. Li, Y. P. Wu, and H. Q. Wu, *Electrochem. Commun.*, 2006, **8**, 1553.
- 43 H. Li, Z. H. Chen, C. K. Tsang, Z. Li, X. Ran, C. Lee, B. Nie, L. X. Zheng, T. Hung, J. Lu, B. Pan and Y. Y. Li, *J. Mater. Chem. A*, 2014, **2**, 229.
- 44 Z. Q. Yuan, Y. Wang and Y. T. Qian, *RSC Advances*, 2012, **2**, 8602.
- 45 C. Z. Yuan, X. G. Zhang, L. H. Su, B. Gao and L. F. Shen, *J. Mater. Chem.*, 2009, **19**, 5772.

## TOC



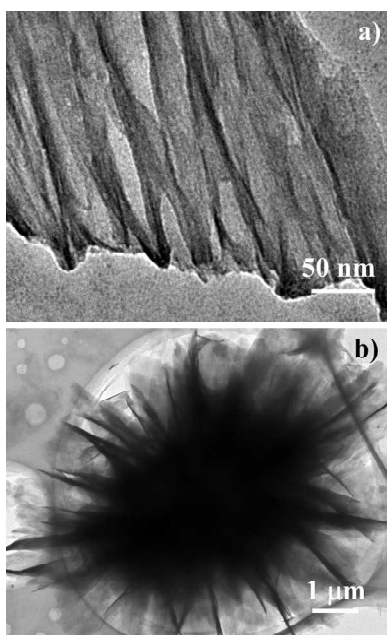
Layered structure Zn-doped Ni-MOF was firstly used as the electrode material for a supercapacitor and exhibited a large specific capacitance of  $1620 \text{ F g}^{-1}$  at  $0.25 \text{ A g}^{-1}$ .

## Supporting Information

**Zn-doped Ni-MOF material with a high supercapacitive performance**Jie Yang,<sup>a, b</sup> Cheng Zheng<sup>a, b</sup> Peixun Xiong,<sup>a, b</sup> Yafeng Li<sup>a, b</sup> and Mingdeng Wei<sup>\*a, b</sup><sup>a</sup> State Key Laboratory of Photocatalysis on Energy and Environmet, Fuzhou University, Fuzhou, Fujian 350002, China<sup>b</sup> Institute of Advanced Energy Materials, Fuzhou University, Fuzhou, Fujian 350002, China

\*Corresponding author: Mingdeng Wei

Tel./fax: +86-591-83753180

*E-mail address:* [wei-mingdeng@fzu.edu.cn](mailto:wei-mingdeng@fzu.edu.cn)**Fig. S1** TEM images of Zn-doped Ni-MOF materials: (a) MOF-0 and (b)MOF-2.

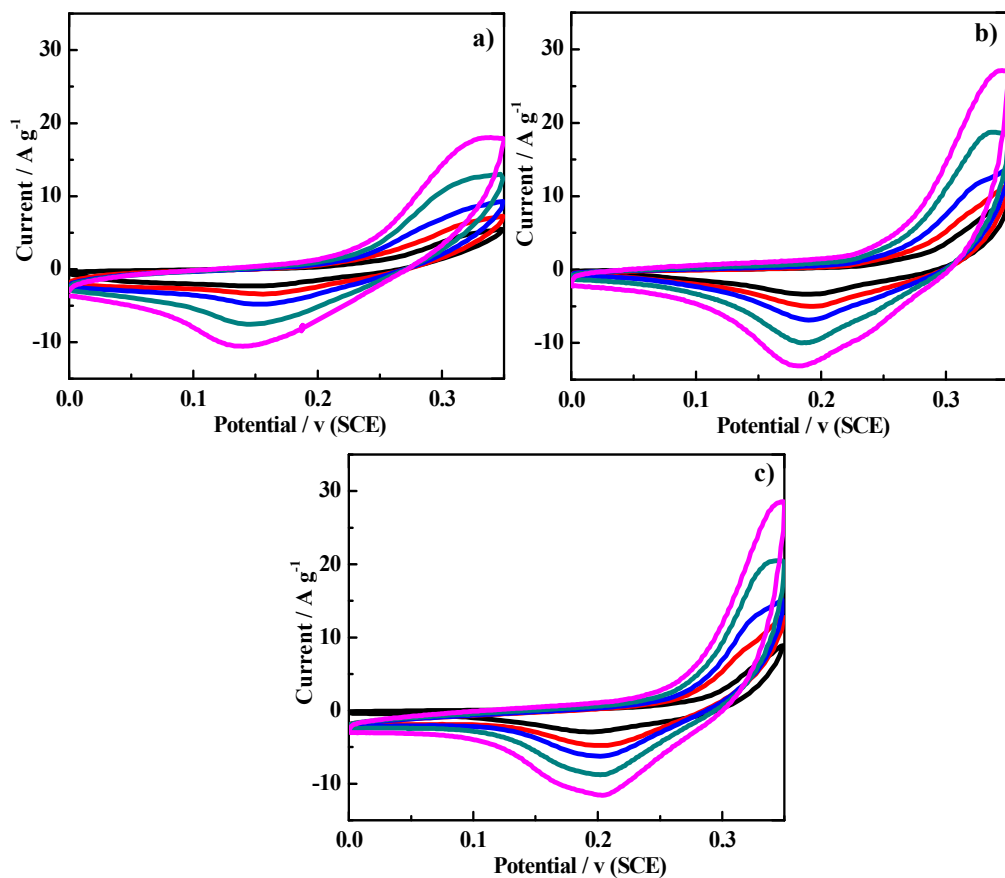


**Fig.S2** CV curves of Zn-doped Ni-MOF materials: (a) MOF-0, (b) MOF-1 and (c) MOF-3.

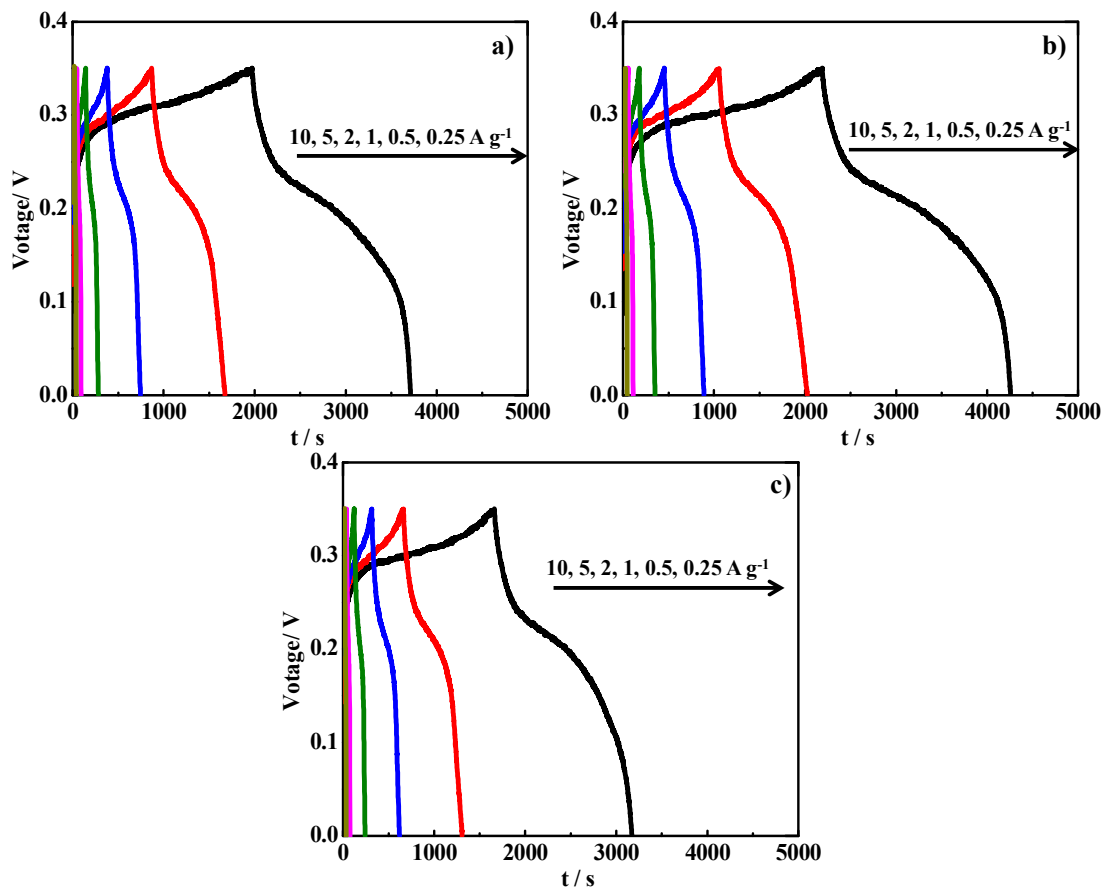
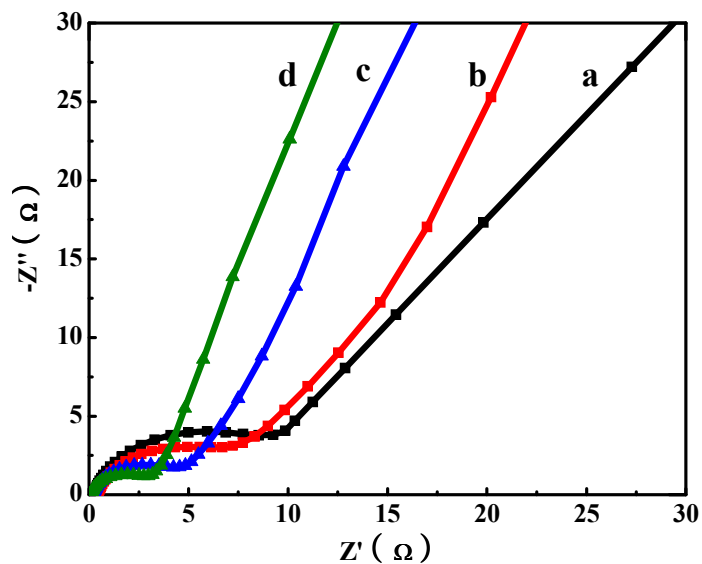
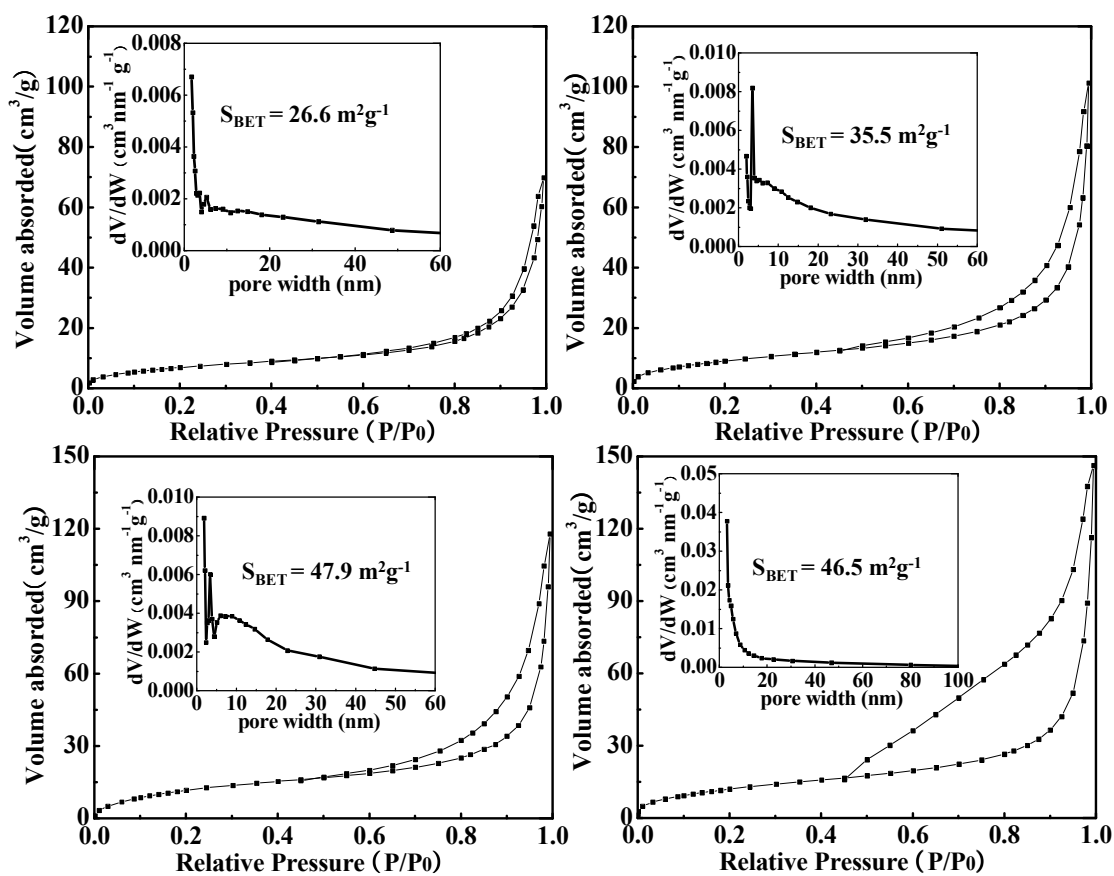


Fig. S3 Charge-discharge profiles of Zn-doped Ni-MOF materials: (a) MOF-0, (b) MOF-1 and (c) MOF-3.



**Fig.S4** EIS plots of Zn-doped Ni-MOF materials: (a) MOF-0, (b) MOF-1, (c) MOF-2 and (d) MOF-3.



**Fig. S5** N<sub>2</sub> adsorption-desorption isotherms and the pore size distribution curves for Zn-doped Ni-MOF materials : (a) MOF-0, (b) MOF-1, (c) MOF-2 and (d) MOF-3.

**Table S1** The interplanar spacing variation for different Zn-doped Ni-MOF materials.

spacing	MOF-0	MOF-1	MOF-2	MOF-3
$d_{(100)} / \text{nm}$	0.953	1.027	1.037	1.040
$d_{(2-10)} / \text{nm}$	0.482	0.555	0.576	0.581

**Table S2** The wavenumber variation for different Zn-doped Ni-MOF materials.

wavenumber	MOF-0	MOF-1	MOF-2	MOF-3
$\nu_{as}(\text{COO}^-) / \text{cm}^{-1}$	1572	1574	1578	1583
$\nu_s(\text{COO}^-) / \text{cm}^{-1}$	1383	1381	1378	1372
$\Delta_\nu / \text{cm}^{-1}$	189	193	200	211